Journal of Solid State Chemistry 184 (2011) 3357–3363

Contents lists available at SciVerse ScienceDirect

Journal of Solid State Chemistry

journal homepage: www.elsevier.com/locate/jssc

A practical grinding-assisted dry synthesis of nanocrystalline $NiMoO_4$ polymorphs for oxidative dehydrogenation of propane

Miao Chen [a,b,*], Jia-Ling Wu [a], Yong-Mei Liu [a], Yong Cao [a,*], Li Guo [b], He-Yong He [a], Kang-Nian Fan [a]

[a] Shanghai Key Laboratory of Molecular Catalysis and Innovative Materials, Department of Chemistry, Fudan University, Shanghai 200433, PR China
[b] Zhejiang Chemical Industry Research Institute, Hangzhou 310023, PR China

ARTICLE INFO

Article history:
Received 20 April 2011
Received in revised form
25 August 2011
Accepted 16 October 2011
Available online 21 October 2011

Keywords:
$NiMoO_4$
Nanocrystalline
Grinding
Propane
Oxidative dehydrogenation

ABSTRACT

A practical two-stage reactive grinding-assisted pathway waste-free and cost-effective for the synthesis of $NiMoO_4$ has been successfully developed. It was demonstrated that proper design in synthetic strategy for grinding plays a crucial role in determining the ultimate polymorph of $NiMoO_4$. Specifically, direct grinding (DG) of MoO_3 and NiO rendered α-$NiMoO_4$ after annealing, whereas sequential grinding (SG) of the two independently pre-ground oxides followed by annealing generated β-$NiMoO_4$ solid solution. Characterizations in terms of Raman and X-ray diffraction suggest the creation of β-$NiMoO_4$ precursor in the latter alternative is the key aspect for the formation of β-$NiMoO_4$. The DG-derived α-$NiMoO_4$ tested by oxidative dehydrogenation of propane exhibited superior activity in contrast to its analog synthesized via conventional coprecipitation. It is suggested that the favorable chemical composition facilely obtained via grinding in contrast to that by coprecipitation was essential for achieving a more selective production of propylene.

1. Introduction

Catalysts based on nickel molybdates have been employed in a wide variety of industrial processes, such as hydrodesulfurization, hydrodenitrogenation, water-gas shift reaction, steam reforming, and other industrially important hydrogenation and hydrotreating reactions [1]. In the last few decades, it has been also well established that $NiMoO_4$-containing materials are promising candidates for the selective oxidation dehydrogenation (ODH) of light alkanes [2–6]. In this field, tremendous efforts have been dedicated to further promote the ODH performance of Ni–Mo–O materials, consequently parameters including preparation techniques [7], support effect [3], and additives [8,9] have been extensively studied. With respect to the preparation of $NiMoO_4$, synthetic approaches including coprecipitation [10], sol–gel [11], reactive sputtering [12], combustion synthesis [13], etc. have been reported, among which coprecipitation is to date the most prevailing in synthesis of $NiMoO_4$ as catalyst [1]. However, lack of reproducibility in chemical composition as well as catalytic results presents as the most unsatisfactory aspect for coprecipitation. Hence, rigorous control of a set of parameters (ratio Ni:Mo/pH/temperature/concentration) during the whole procedure is often implemented to ensure the expected chemical composition [10]. Such operations, strict and tedious as they are, significantly complicate the synthetic process. Moreover, the wet synthesis adds to environmental pressure by producing tremendous wastes. In this context, development of new practical, efficient, and environmentally friendly methods for the preparation of the multicomponent $NiMoO_4$-based catalyst system is highly desired.

Reactive grinding based on mechanochemical activation has long been known as an approach successfully applied in the synthesis of various metal alloys and nanostructured metal-oxide phases [14–20]. This method was also applied to the alloying of such brittle materials as Si and Ge [21], to the synthesis of composite materials incorporating preformed oxide or carbide particles into a metallic matrix [18] or to the nitrogenation of iron or steel under nitrogen or ammonia [22]. The highly nonequilibratory nature of the grinding process may provide a unique opportunity to prepare catalytic materials with improved and/or novel physical and chemical properties [23–25]. Another attractive aspect of grinding is its extreme simplicity and absence of residues. Typically, the solid-state reaction includes two major steps: (i) mixing and milling of the two oxides; and (ii) calcination which results in further chemical interaction [26]. In contrast to coprecipitation, solid state reaction in preparing $NiMoO_4$ may significantly lower the demand for strict control of a series of experimental parameters. In view of the above-mentioned unique properties, reactive grinding may be of high potential in

* Corresponding author at: Shanghai Key Laboratory of Molecular Catalysis and Innovative Materials, Department of Chemistry, Fudan University, Shanghai 200433, PR China.
E-mail addresses: chenmiao@sinochem.com (M. Chen), yongcao@fudan.edu.cn (Y. Cao).

0022-4596/$ - see front matter © 2011 Elsevier Inc. All rights reserved.
doi:10.1016/j.jssc.2011.10.024

practically fabricating and modifying nickel molybdate materials starting from corresponding simple oxides in order to achieve high and reproducible ODH performance.

In an earlier study, Mamoru et al. have synthesized $NiMoO_4$ efficiently through grinding-assisted solid state reaction starting from NiO and MoO_3, and have analyzed the formation rate of $NiMoO_4$ either in a separate or in mixed grinding [27]. However, study in the impact of grinding strategy on crystalline structure and catalytic activity of $NiMoO_4$ has not been performed. In the present study, we also employ the method of waste-free and cost-effective grinding activation in the preparation of nickel molybdates catalysts from NiO and MoO_3. Two different strategies in grinding, namely direct grinding and sequential grinding, have been proposed and adopted in the manufacture of nickel molybdate with α- and β-crystalline forms, respectively. Probe reaction by ODH of propane has been employed to determine the catalytic activity of the grinding-derived $NiMoO_4$, and further compare with that of its analog synthesized via traditional coprecipitation. The Ni–Mo–O samples submitted to thermal processing at various temperatures as well as their as-ground precursors were characterized by X-ray diffraction (XRD), Raman, X-ray photoelectron spectroscopy (XPS) and BET techniques, and these results were carefully analyzed to account for the ODH performance and the mechanism with respect to the formation of different $NiMoO_4$ polymorphs.

2. Experimental

2.1. Catalyst preparation

Two different grinding strategies including direct and sequential activation of equimolar mixture of NiO (Aldrich, 99%) and MoO_3 (Aldrich, 99%) during the grinding procedure were employed for the preparation of nanocrystalline $NiMoO_4$. The milling was performed in a high energy planetary ball mill (model QM-1SP04), using a rotational speed of 300 rpm at a constant rotation direction and a ball to powder weight ratio of 20:1. Both the vial (50 mL) and the balls (4–6 mm) were made of stainless steel. Direct grinding (DG) refers to grinding of crude NiO and MoO_3 together for 4 h, and sequential grinding (SG) refers to pre-grinding for 2 h of the two oxides separately followed by mixing and further grinding for another 2 h. The precursors resulting from the direct or sequential grinding were then subjected to annealing at elevated temperatures (400 and 600 °C) for 4 h in air, and were denoted as DG-T or SG-T (T represents the calcination temperature), respectively. For comparison, a reference sample (CP-600) was prepared by a conventional coprecipitation method [10]. In brief, nickel nitrate solution (0.25 M) was added to an equimolar 0.25 M molybdic acid solution at 85 °C, and then the pH was adjusted to 5.25 by dropwise addition of ammonia. The precipitate obtained was hot-filtered and dried at 120 °C for 15 h, followed by calcination at 600 °C for 4 h.

2.2. Catalyst characterization

XRD were collected using a Germany Bruker D8Advance X-ray diffractometer equipped with a graphite monochromator, operating at 40 kV and 40 mA and employing nickel-filtered Cu-$K\alpha$ radiation ($\lambda=1.5406$ Å). Laser Raman spectra were obtained using a confocal microprobe Jobin Yvon Lab Ram Infinity Raman. The visible Raman measurements were carried out using internal Ar^+ excitation at 514.5 nm with a power of approximately10 mW. The BET specific surface areas were measured on a Micromeritics TriStar 3000 apparatus. XPS spectra were recorded with a Perkin-Elmer PHI 5000C system equipped with an hemispherical electron energy analyzer. The spectrometer was operated at 15 kV and 20 mA, and a magnesium anode (Mg $K\alpha$, $h\upsilon=1253.6$ eV) was used. The background pressure during data acquisition was maintained at $<2.0\times10^{-5}$ Pa. The C 1*s* line (284.5 eV) was used as the reference to calibrate the binding energies (B.E.). Transmission electron microscopy (TEM) images were recorded digitally on a JEOL 2011 electron microscope operating at 200 kV.

2.3. Reaction tests

The catalysts were tested in a fixed-bed, quartz tubular stem-flow reactor (i.d. 4 mm, length 400 mm) operated at atmospheric pressure. The reactor was equipped with a coaxial thermocouple for catalytic bed temperature monitoring. 100 mg catalyst sample (60–80 mesh) was introduced into the reactor and diluted with 150 mg quartz powder (40–60 mesh) to keep a constant volume in the catalyst bed. Prior to reaction the catalyst was pretreated with oxygen under the flow rate of 5 ml/min at 600 °C for 1 h, then heated to 700 °C for 15 min and subsequently cooled down to the reaction temperature. The reaction feed mixture was composed of propane/oxygen/nitrogen at a molar ratio of 1:1:8. The feed and the reaction products were analyzed on-line by online gas chromatograph (Type GC-122, Shanghai). Permanent gases (N_2, CO, CO_2) were separated using a TDX-01 column connected to a TCD detector and other reaction products were analyzed employing a Porapak Q column connected to a FID detector. Blank runs show that under the experimental conditions used in this work the homogeneous reaction could be neglected.

3. Results and discussion

The structural evolutions for the two series of ground samples as a function of calcination temperature ranging from 400 °C to 600 °C have been followed by XRD, and the results are shown in Fig. 1. With respect to the as-ground samples, the diffraction lines broad and weak assignable to both NiO and MoO_3 were observed (Fig. 1a). Since fresh NiO and MoO_3 are with very strong diffraction signals (not shown), it is clear that grinding (either DG or SG) plays a major role in decreasing the crystallinity of both oxides. After calcination at 400 °C (Fig. 1b), the DG-400 sample still shows signals ascribed exclusively to NiO and MoO_3, and with apparently stronger intensities. On the other hand, SG-400 exhibits a series of new characteristic peaks ($2\theta=26.7°$, 28.7°, 33.4°, etc.) in addition to those of simple oxides. These new peaks are assigned to a β-$NiMoO_4$-like phase. Similar observation of β-$NiMoO_4$ was reported by Moreno et al. by combustion–synthesis of Ni–Mo–O material, as exists either in the as-prepared stage or after calcination at 350 °C in air [13]. It should be ponited out that pure β-$NiMoO_4$ is a metastable phase, which exists *in-situ* at high temperature, and transition from polymorph α to β usually completes at above 700 °C. Reversely, cooling to below 200 °C allows conversion from β- back to α-$NiMoO_4$ [28]. However, a specific type of solid solution of β-$NiMoO_4$ with small fraction of NiO, which closely resembles β-$NiMoO_4$ in structure, is reported to be stable at ambient condition. Note that the 2θ value of the strongest diffraction line (220) for SG-400 is 26.7° (Fig. 1), slightly higher than that for normal β-$NiMoO_4$ (26.4°), yet fits well with that of β-$NiMoO_4$ in the solid solution form [1]. In other words, sample SG-400 actually comprises β-$NiMoO_4$ solid solution together with simple oxides of NiO and MoO_3.

Calcination at 600 °C rendered prominent modifications in phase composition: no information regarding simple oxides was observed for both DG-600 and SG-600, and the well-defined diffraction peaks (2θ at 14.3°, 25.3°, 28.8°, 32.6°, 43.9°, 47.4°, etc.) were identified for DG-600. These new diffraction peaks are

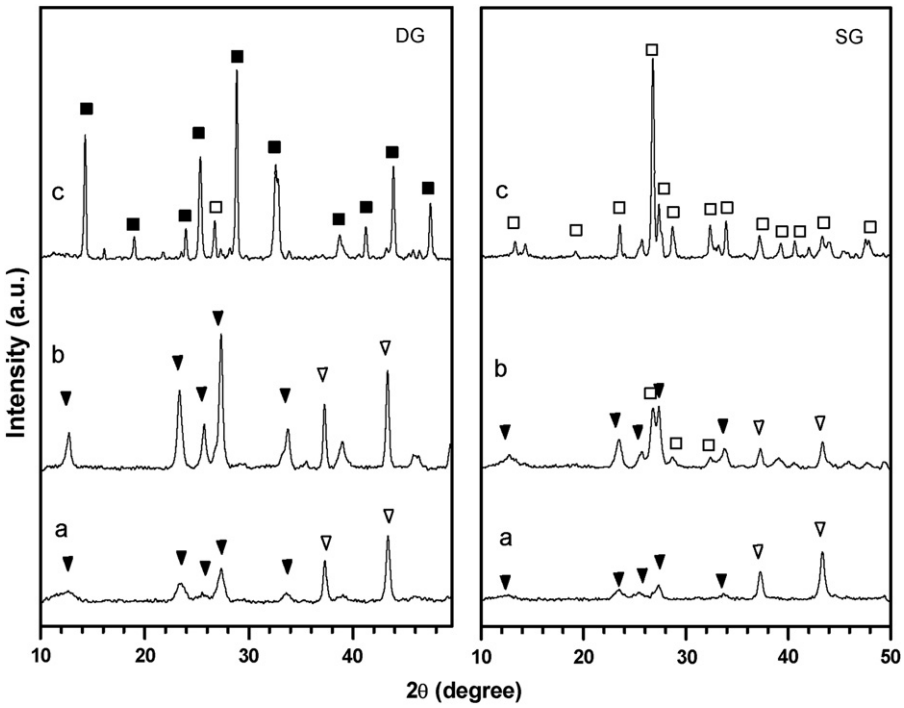

Fig. 1. XRD profiles for the as-ground Ni–Mo–O samples and those calcined at different temperatures: (a) as ground, (b) 400 °C, and (c) 600 °C. (■) α-$NiMoO_4$; (□) β-$NiMoO_4$; (▼) MoO_3; and (▽) NiO.

attributable to α-$NiMoO_4$ [29], suggesting 600 °C is a temperature permitting solid state reaction of simple oxides that generate α-$NiMoO_4$. This fact is in line with the result by Neiman et al. on simple solid state synthesis of α-$NiMoO_4$ [30], and the solid state preparation based on grinding in this work offers a even higher conversion of NiO and MoO_3. As for the SG-600 sample, signals assigned exclusively to β-$NiMoO_4$ (in a solid solution form) crystalline structures were observed, suggesting approximately full transformtion of NiO and MoO_3 to β-$NiMoO_4$ solid solution occurred after annealing up to 600 °C. β-$NiMoO_4$ supported on TiO_2 previously has also been obtained via impregnation and coprecipitation method after calcination at 550 °C by Zavoianu et al. [29]. Nevertheless, rather than the approximately exclusive formation of α- or β-$NiMoO_4$ for DG-600 and SG-600, respectively, coexistence of α- and β-$NiMoO_4$ was present in these impregnation/coprecipitation-derived samples. In this work, through comparison of the results of DG-600 and SG-600, it is clear that the employment of strategy for grinding is crucial that determines the specific ploly-morph of $NiMoO_4$ after calcination at 600 °C.

To gain insight into the mechanisic interpretation for the development of nickle molydate, Raman was employed to investigate the structural information with respect to the as-ground precursor for DG and SG, as well as those calcined at 400 °C and 600 °C, respectively. As shown in Fig. 2, for all samples signals assigned to NiO were not identified, owing to the inherent nature that even if well-crystallized NiO provides ill-defined Raman spectrum [31]. On the other hand, bands centering at 991, 818, 662, 374, 332, and 281 cm^{-1} were detected for all the as-ground precusors, and were attributable to viberation modes of MoO_3 [32]. Prolonged grinding time allowed weaker signals of MoO_3 for DG (Fig. 2a), in agreement with the decreased crystallinity through grinding as revealed by XRD. Through comparison of the precusors of DG and SG, it is interesting to note that an additional band locating at 948 cm^{-1} is observed for SG rather than for DG (designated by dash line in Fig. 2b). After calcination at 400 °C, bands for MoO_3 were with stronger intensities, and the band at 948 cm^{-1} still existed for SG-400 (Fig. 2c). After calcination at 600 °C, two series of bands located at 957, 909, 702 cm^{-1} and 948, 901, 697 cm^{-1}, assignable to α- and β-$NiMoO_4$ [31,33], were observed for DG-600 and SG-600, respecively (Fig. 2d). Coincident with the strongest band for SG-600, the band at 948 cm^{-1} for SG-400 and the SG precursor should possibly be assigned to β-$NiMoO_4$. This implies "β-$NiMoO_4$" (probably in a solid solution form) readily exists in the precursors for SG instead of DG. This type of β-$NiMoO_4$ may be of small grain size, for it cannot be detected by XRD. In a study by Moreno et al. on combustion synthesis of β-$NiMoO_4$, similar "β-$NiMoO_4$" species (probably with larger particle size, as detected by XRD) was present in the as-prepared sample before calcination [13]. Attempt was further made to observe this type of β-$NiMoO_4$ over the as-ground SG sample via TEM. Unfortunately, the β-$NiMoO_4$ cannot be identified due to the extremely poor contrast between the amorphous species which had been heavily ground (not shown).

On considering the crystalline structures of NiO and MoO_3, it is known that well-crystallized and amorphous MoO_3 comprise six-coordinated MoO_6 octahedra and four-coordinated MoO_4 tetrahedra, respectively [34], while NiO_6 octahedra presents as the exclusive crystalline unit for NiO in both cases (Scheme 1) [35]. As for the structure of α- and β-$NiMoO_4$, α-$NiMoO_4$ is composed of infinite chains of edge-sharing NiO_6 and MoO_6 octahedra, while β-$NiMoO_4$ comprises alternatively connected NiO_6 octahedra and MoO_4 tetrahedra [36]. During grinding, according to Trovarelli et al., the ball–powder–ball collisions permit the continuous breaking and formation of chemical bonds, and local temperature of the being milled powders rises and local surface melts [20]. Hence, new species is likely formed via high-energy collisions between Ni–O and Mo–O polyhedrons as well as local heating on the contacts during reactive grinding. One should keep in mind that amorphous as well as defect-rich NiO (comprises NiO_6 octahedra) and MoO_3 (comprises MoO_4 tetrahedra) thrive during grinding, in view of their sharply decreased crystallinity as evidenced by XRD. This result, together with their crystalline structures, suggest that it may be the Ni–O–Mo bond formation

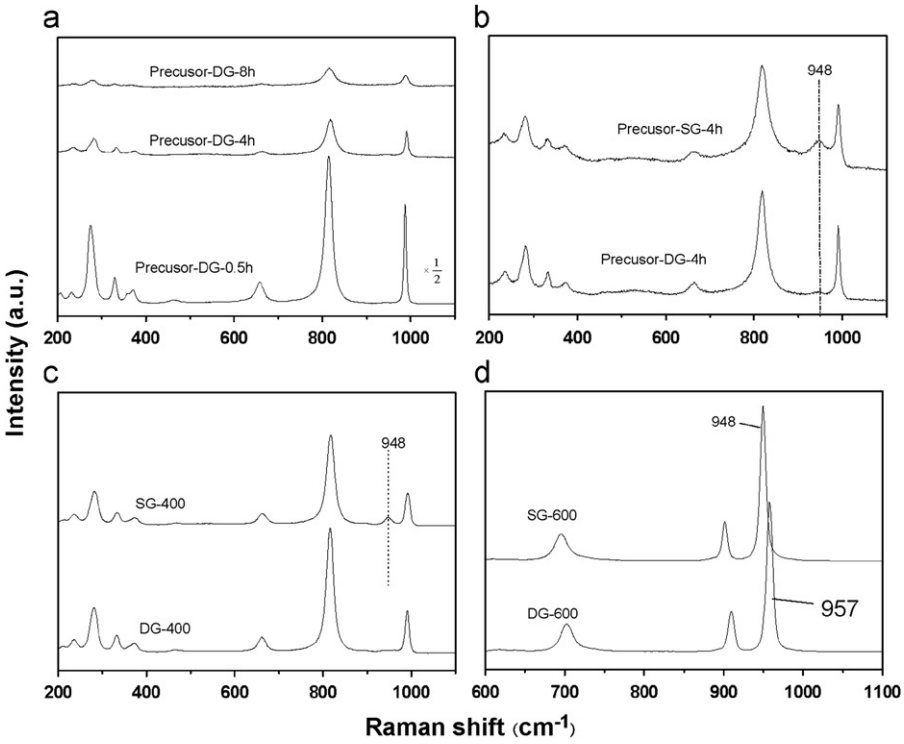

Fig. 2. Raman spectra for (a) DG precursors with grinding time at 0.5, 4 and 8 h; (b) DG and SG precursors ground for 4 h; (c) DG-400 and SG-400; and (d) DG-600 and SG-600.

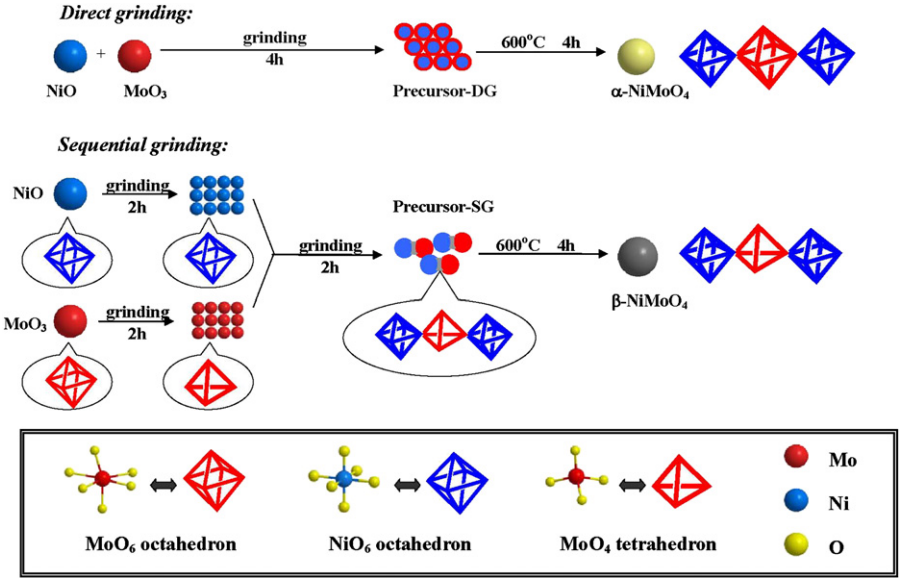

Scheme 1. Mechanistic illustration for DG- and SG-assisted synthesis with respect to structural evolutions for the Ni–Mo–O samples.

between NiO_6 octahedra and MoO_4 tetrahedra in solid state reaction that generated "β-$NiMoO_4$" (illustrated in Scheme 1).

It has been well established that molybdenum oxide exhibits a layered structure, which indicates the existence of weak interlayer and strong intralayer bonding that allows MoO_3 a high surface mobility [34]. As a consequence, when dispersing along the product surface (MoO_3–MeO_x; *Me*=Cd, Ni, Pb, etc.), MoO_3 always forms a surface adsorption phase (Mo–O–s) with the surface molar ratio of Mo/*Me* > 1 [30]. One can imagine an inhibition of the desired Ni–O–Mo bond formation once far excessive MoO_3 accumulates on the external surface of the ground particles, since intimate contact between different reactants on the particle's superficial layers is a prerequisite. XPS was performed to study the surface composition of the as-ground Ni–Mo–O precursors. Notice that the surface Mo/Ni molar ratios for DG is 4.8 (Table 1), obviously far from stoichiometric. Namely, the external surface for the ground sample is predominantly covered by MoO_3, which may well account for the scarce creaction of the β-$NiMoO_4$ precursor during DG. With respect to SG, on the other hand, NiO_6 octahedra and MoO_4 tetrahedra were abundantly created via the separate-grinding procedure, free from mutual covering. Subsequently, the together-grinding procedure offers adequate opportunity for connection between NiO_6 octahedra and MoO_4 tetrahedra, which consequently generates the unit for β-$NiMoO_4$. Since NiO_6 octahedra and MoO_4 tetrahedra are building

Table 1
Physicochemical information for DG-600, SG-600 and CP-600.

Catalyst	S_{BET} (m^2/g)	Mo/Ni[a] (±0.1)	Mo/Ni[b] (±0.1)	Lattice parameters				
				a (Å) (±0.01)	b (Å) (±0.01)	c (Å) (±0.01)	β (deg.)	V (Å^3) (±1)
DG-600	7.6	4.8	1.1	9.51	8.81	7.66	114	588
SG-600	11.6	2.8	1.1	10.1	9.12	6.99	106	621
CP-600	54.0	–	0.75	9.52	8.81	7.66	114	588

[a] Surface Mo/Ni molar ratio for as-ground precursors calculated from XPS.
[b] Surface Mo/Ni molar ratio for annealed catalysts calculated from XPS.

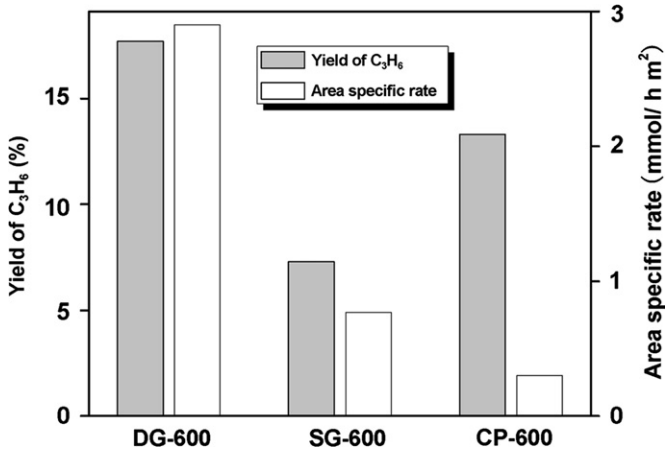

Fig. 3. Yield and area specific rate of propylene for DG-600, SG-600 and CP-600, reaction temperature=600 °C, $C_3H_8/O_2/N_2$=1:1:8, GHSV=11,900 h^{-1}.

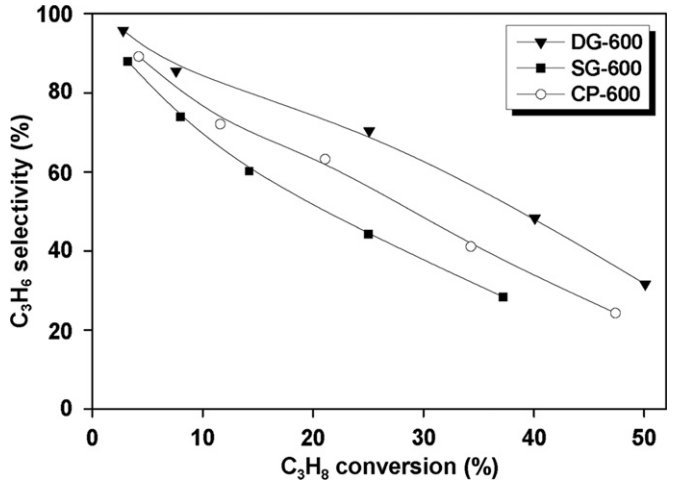

Fig. 4. Selectivity to C_3H_6 versus the conversion of C_3H_8 for DG-600, SG-600 and CP-600, reaction temperature=600 °C, $C_3H_8/O_2/N_2$=1:1:8.

blocks for β-$NiMoO_4$, SG not only fabricates them, but also allows their effective assembly to the target product. This may explain why "β-$NiMoO_4$" is preferentially created during SG rather than DG. Through further calcination, the thus-obtained β-$NiMoO_4$ precursor performs as the crystalline seed that induces generation of a higher population of as well as better-crystallized β-$NiMoO_4$ (in a solid solution form).

As far as application is concerned, it is important to test the catalytic activity of the grinding-derived $NiMoO_4$ samples. Selective ODH of propane to propylene has been employed as the probe reaction, given its economic significance as to upgrading cheaper paraffin feedstock into value-added olefin as the important industrial raw materials [37,38]. The activity results of DG-600 and SG-600 were shown in Fig. 3, along with sample CP-600 used as a reference. As should be pointed out, phase-pure β-$NiMoO_4$ is believed as the more selective form of nickel molybdate for ODH [1]. In this sense, the heat treatment up to 700 °C for 0.25 h prior to the reaction test is commonly employed, which is aimed at *in-situ* transforming the possible α-$NiMoO_4$ to β-$NiMoO_4$ [5,6]. Under this circumstance, at 600 °C and GHSV=11,900 h^{-1}, the yield of propylene is observed to follow the sequence: DG-600 > CP-600 > SG-600 (Fig. 3). The lowest activity for SG-600 is not surprising, since solid solutions of NiO and β-$NiMoO_4$ were reported to be with inferior ODH activity in contrast to simple α- or β-$NiMoO_4$ [1]. On the other hand, DG-600, compared favorably with CP-600 and SG-600, is with the maximum yield of propylene (17.8%). If calculated in term of area specific rate (mmol/h m^2), activity of DG-600 appears to be an order of magnitude higher than that for CP-600 (Fig. 3). Fig. 4 shows the selectivity to propylene for DG-600, SG-600 and CP-600 as a function of propane conversion at 600 °C. For all catalysts, selectivity to propylene decreases with increasing the propane conversion over the range of propane conversion investigated (*c.a.* 3–50%). For a given propane

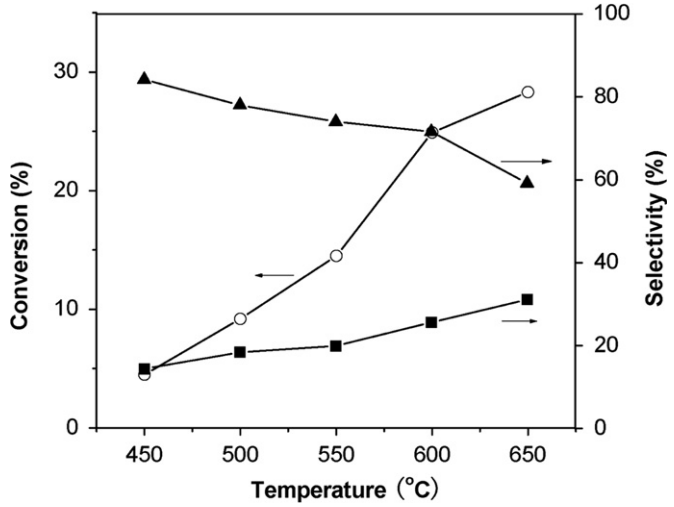

Fig. 5. Propane conversion (○), selectivity to propylene (▲) and carbon oxides ($CO+CO_2$) (■) as a function of temperature for DG-600, $C_3H_8/O_2/N_2$=1:1:8, GHSV=11,900 h^{-1}.

conversion, DG-600 exhibits obviously higher selectivity to propylene than the other two counterparts.

To account for the superior catalytic results achieved over the DG sample, calculation on crystalline parameters for DG-600, CP-600 and SG-600 were carried out, since lattice defects have been previously suggested as a plausible interpretation to higher activities for $CHClF_2$ dismutation over the ground α-AlF_3 [39]. However, with respect to DG-600 and CP-600 (both with the α-polymorph), no evident discrepancy in lattice parameters was shown (Table 1), excluding lattice defects as the possible explanation. In addition to

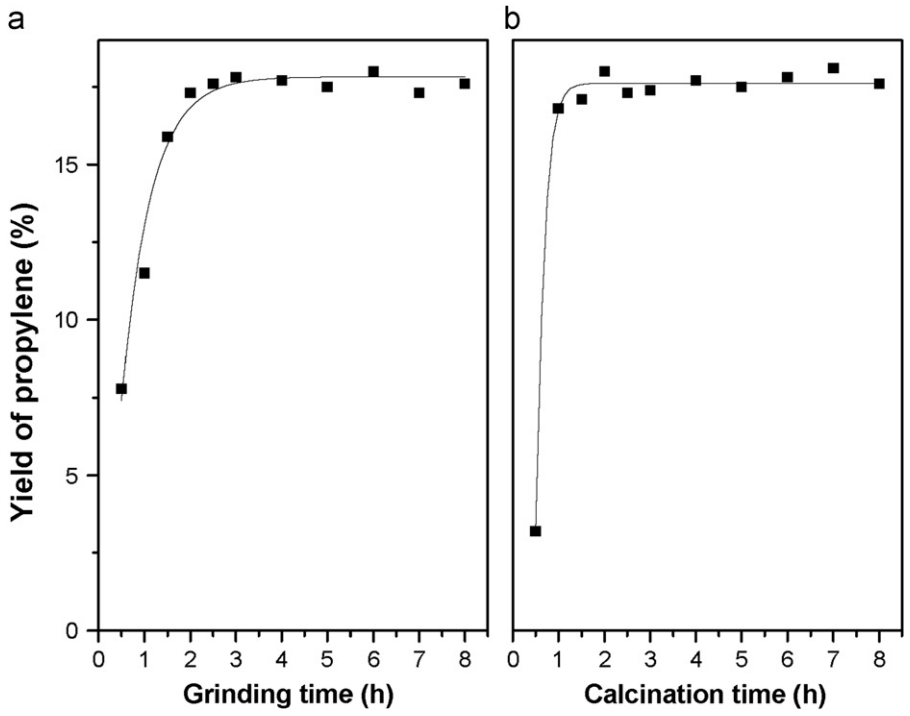

Fig. 6. Yield of propylene as functions of (a) grinding time with calcination at 600 °C for 4 h and (b) calcination time at 600 °C with grinding time for 4 h for DG-600, reaction temperature = 600 °C, $C_3H_8/O_2/N_2$ = 1:1:8, GHSV = 11,900 h^{-1}.

the above-mentioned consideration, excessive NiO on surface is commonly believed to be detrimental for the ODH activity of nickel molybdate, in view of its strong promotion to undesired over-oxidation [1]. The $NiMoO_4$ synthesized via coprecipitation is often inevitably contaminated by NiO, since formation of $Ni(OH)_2$ deposition is available in a far wider pH as well as temperature range than for $NiMoO_4$ [10]. The XPS analysis reveals approximately stoichiometric Mo/Ni ratio for DG-600 and SG-600, whereas slightly surplus NiO for CP-600 (Table 1). Therefore, it should be the favorable chemical composition facilely achieved on the DG-600 surface that well accounted for its superior activity in contrast to that of CP-600.

In order to study the effect of reaction temperature on activity for DG-600, the ODH was tested in the reaction temperature range of 400–650 °C. The conversion of propane increased monotonously from 4.5% to 28.3% as the temperature increased from 400 to 650 °C (Fig. 5). On the other hand, the consecutive over-oxidation of hydrocarbons to carbon oxides is more severe at higher temperature, as the selectivity to CO_x amounts to 31.1% for at 650 °C. Taking both the selectivity to propylene and conversion of propane into account, 600 °C is the temperature of choice, which provides a maximum yield of propylene at 17.8%. This result is closely comparable with to date the highest ODH result reported by Mazzocchia et al. (with yield of propylene at 18.1%) over unsupported $NiMoO_4$ at 600 °C [40].

To gain further insights into the reproducibility of the active catalytic results for the grinding-synthesized samples, the dependences of propylene yield on grinding time and calcination time for DG-600 were investigated, respectively. By varying the grinding time from 0.5 to 8 h, followed by calcination at 600 °C for 4 h, it is shown that high yield of propylene at *c.a.* 17% has always been obtained with grinding for over 2 h (Fig. 6a). On the other hand, with fixed grinding time at 4 h, calcination for over 1.5 h ensures high production of propylene (Fig. 6b). The above results clearly demonstrate the excellent repeatability for grinding in achieving catalytic active $NiMoO_4$. Therefore, all the above mentioned merits including simplicity in operation, flexibility in tuning polymorph structure, high catalytic performance, and good reproducibility, combined that allows grinding to be not only a potentially practical route for the synthesis of nickel molybdates, but also a promisingly extended alternative for manufactures of a variety of other important multi-component systems.

4. Conclusions

In summary, we have shown that grinding-assisted activation of equimolar NiO and MoO_3 followed by thermal processing allows for the facilely waste-free fabrication of nanocrystalline $NiMoO_4$ materials. To be versatile, select of properly designed grinding strategies in terms of DG and SG led to formations of $NiMoO_4$ with α- and β- polymorphs, respectively. By adopting SG, β-$NiMoO_4$ solid solution was obtained at below 700 °C, owing to the achievement of β-$NiMoO_4$ precursor via solid state reaction. The DG preparation of α-$NiMoO_4$ sample, highly effective for the ODH of propane, was shown to be with good reproducibility. The superior performance for the grinding-derived α-$NiMoO_4$ nanocrystals, in contrast to its analog obtained by conventional coprecipitation, has been attributed to the favorable creation of α-$NiMoO_4$ that free from contamination of NiO. This new approach may offer an attractive alternative for the convenient synthesis of other important multicomponent catalyst systems with controlled compositions and structures.

Acknowledgments

This work was financially supported by the National Natural Science Foundation of China (20873026 and 21073042), New Century Excellent Talents in the University of China (NCET-09-0305), the National Basic Research Program of China (2009CB623506), and Science & Technology Commission of Shanghai Municipality (08DZ2270500).

References

[1] L.M. Madeira, M.F. Portela, C. Mazzocchia, Catal. Rev. 46 (2004) 53–110.
[2] U. Ozkan, G.L. Schrader, J. Catal. 95 (1985) 137–146.
[3] R. Zvoianu, C.R. Dias, A.P.V. Soares, M.F. Portela, Appl. Catal. A 298 (2006)40-49 298 (2006).
[4] F. Dury, E.M. Gaigneaux, P. Ruiz, Appl. Catal. A 242 (2003) 187–203.
[5] M. Sautel, G. Thomas, A. Kaddouri, C. Mazzocchia, R. Anouchinsky, Appl. Catal. A 155 (1997) 217–228.
[6] D.L. Stern, R.K. Grasselli, J. Catal. 167 (1997) 550–559.
[7] U. Ozkan, G.L. Schrader, J. Catal. 95 (1985) 120–136.
[8] L.M. Madeira, R.M. Martin-Aranda, F.J. Maldonado-Hodar, J.L.G. Fierro, M.F. Portela, J. Catal. 169 (1997) 469–479.
[9] R.M. Martin-Aranda, M.F. Portela, L.M. Madeira, F. Freire, M. Oliveira, Appl. Catal. A 127 (1995) 201–217.
[10] C. Mazzocchia, R. Anouchinsky, A. Kaddouri, M. Sautel, G. Thomas, J. Therm. Anal. 40 (1993) 1253–1265.
[11] P. Courty, H. Ajot, C. Marcilly, B. Delmon, Powder Technol. 7 (1973) 21–38.
[12] J.Y. Zou, G.L. Schrader, Study Surf. Sci. Catal. 82 (1994) 19–26.
[13] B. Moreno, E. Chinarro, M.T. Colomer, J.R. Jurado, J. Phys. Chem. C 144 (2010) 4251–4257.
[14] V. Sepelák, I. Bergmann, S. Indris, J. Subrt, P. Heitjans, K.-D. Becker, AIP Conf. Proc. 1258 (2010) 96–101.
[15] V.V. Boldyrev, Russ. Chem. Rev. 75 (2006) 177–189.
[16] C. Suryanarayana, E. Ivanov, V.V. Boldyrev, Mater. Sci. Eng. A 304–306 (2001) 151–158.
[17] V.V. Boldyrev, K. Tkacova, J. Mater. Synth. Process. 8 (2000) 121–132.
[18] E. Gaffet, M. Abdellaoui, N. Malhouroux-Gaffet, Mater. Trans. JIM 36 (1995) 198–209.
[19] D.A. Bulushev, L. Kiwi-Minsker, V.I. Zaikovskii, A. Renken, J. Catal. 193 (2000) 145–153.
[20] A. Trovarelli, F. Zamar, J. Llorca, C. deLeitenburg, G. Dolcetti, J.T. Kiss, J. Catal. 169 (1997) 490–502.
[21] R.M. Davis, C.C. Koch, Scr. Metall. 21 (1987) 305–310.
[22] A. Calka, D. Wexler, J. Zhou, D. Dunne, Mater. Sci. Forum 269–272 (1998) 265–270.
[23] R.A. Buyanov, V.V. Molchanov, V.V. Boldyrev, Catal. Today 144 (2009) 212–218.
[24] R.A. Buyanov, V.V. Molchanov, V.V. Boldyrev, KONA 27 (2009) 38–54.
[25] S. Kaliaguine, A. Van Neste, V. Szabo, J.E. Gallot, M. Bassir, R. Muzychuk, Appl. Catal. A 209 (2001) 345–358.
[26] L.-C. Wang, Y.-M Liu, M. Chen, Y. Cao, H.-Y. He, G.-S. Wu, W.-L. Dai, K.-N. Fan, J. Catal. 246 (2007) 193–204.
[27] S. Mamoru, K. Hiroshi, J. Jpn. Soc. Powder Powder Metall. 30 (1983) 6–11.
[28] A. Kaddouri, R. Del Rosso, C. Mazzocchia, D. Fumagalli, J. Therm. Anal. 63 (2000) 267–277.
[29] R. Zavoianu, C.R. Dias, M. Farinha Portela, Catal. Commun. 2 (2001) 37–42.
[30] A. Neiman, E. Tsipis, I. Beketov, Y. Kotov, A. Murzakaiev, O. Samatov, Solid State Ionics 177 (2006) 403–410.
[31] P. Dufresne, E. Payen, J. Grimblot, J.P. Bonnelle, J. Phys. Chem. 85 (1981) 2344–2351.
[32] B. Samaranch, P. Ramirez de la Piscina, G. Clet, M. Houalla, N. Homs, Chem. Mater. 18 (2006) 1581–1586.
[33] A. Kaddouri, E. Tempesti, C. Mazzocchia, Mater. Res. Bull. 39 (2004) 695–706.
[34] G. Mestl, T.K.K Srinivasan, H. Knozinger, Langmuir 11 (1995) 3795–3804.
[35] F. Parmigiani, L. Sangaletti, J. Electron Spectrosc. 98–99 (1999) 287–302.
[36] J.Y. Zou, G.L. Schrader, Thin Solid Films 324 (1998) 52–62.
[37] M.M. Bettahar, G. Costentin, L. Savary, J.C. Lavalley, Appl. Catal. A 145 (1996) 1–48.
[38] R. Grabowski, Catal. Rev. 48 (2006) 199–268.
[39] G. Scholz, R. Konig, J. Petersen, B. Angelow, I. Dorfel, E. Kemnitz, Chem. Mater. 20 (2008) 5406–5413.
[40] C. Mazzocchia, E. Tempesti, C. Aboumrad, US. Patent 5, 086, 032, 1992.